PHYSICAL REVIEW B VOLUME 28, NUMBER 10 15 NOVEMBER 1983

Electronic transport at grain boundaries in silicon

G. C. McGonigal, D. J. Thomson, J. G. Shaw, and H. C. Card
Materials and Devices Research Laboratory, Department of Electrical Engineering, University of Manitoba, Winnipeg, Manitoba R3T 2N2, Canada
(Received 9 April 1982; revised manuscript received 25 October 1982)

An experimental investigation is reported on carrier transport across isolated grain boundaries in large-grain cast silicon material. Continuous interface-state densities in the $(10^{15}-10^{16})$-$m^{-2}\,eV^{-1}$ range are measured for the lower part of the silicon energy gap. The grain-boundary diffusion potentials for this material are shown in some cases to vary appreciably over a single grain-boundary plane; this is thought to be due to a nonuniform spatial distribution of interface charge at the grain boundaries. Numerical calculations by finite-element methods, of the quasi-Fermi-potentials in the vicinity of the grain boundary, suggest that the supply of majority carriers by diffusion to this interface may be the limiting factor controlling their transport. The experiments have consequently been interpreted according to the diffusion model rather than the customary thermionic-emission model of majority-carrier transport across grain boundaries.

I. INTRODUCTION

The transport properties of electrons and holes at grain boundaries in polycrystalline semiconductors is of considerable present interest, both for academic and practical reasons. The grain boundary differs from other semiconductor interface systems in that the orientation but not the crystal structure changes across this interface; this can give rise to behavior which is unique to this type of interface and as such is of scientific importance. Electronic and optical processes at grain boundaries are of current practical importance as a result of their effects on the photovoltaic conversion efficiency of thin-film polycrystalline semiconductor solar cells.[1]

Pioneering work on the characterization of electronic mechanisms at grain boundaries has been carried out recently by Seager and co-workers at Sandia Laboratories.[2-5] These workers have investigated the effects of grain-boundary interface states on the majority carrier transport in *n*-type polycrystalline silicon. From measurements of current-voltage characteristics performed on isolated grain boundaries, they have been able to extract the energy distribution of interface states.

In this paper we present the results of an experimental investigation of transport phenomena at grain boundaries in silicon. The present work differs from the work of Seager *et al.* in several ways.

One difference is that our investigations are of grain boundaries in *p*-type silicon so that the information obtained concerning grain-boundary interface states corresponds to the energy distribution of these states in the lower half of the energy gap, whereas Seager has obtained data for the upper half of the energy gap by using *n*-type silicon samples. We are also studying a somewhat different material: cast silicon from Wacker Chemitronic Ltd. of the "Silso" type as opposed to their case of neutron-transmutation doped polycrystalline chemical-vapor-deposited (CVD) silicon of smaller grain size and higher doping concentration. We further include in our study the cases of both high and low grain-boundary potential barriers. Optical illumination intensity is employed in addition to bias voltage and temperature as experimental parameters. With the exception of some recent work concerning grain-boundary recombination velocity[5] most of the earlier studies involved dark measurements.[2-4]

This paper also provides a departure from previous work in its treatment of the data in terms of a diffusion model of carrier transport at grain boundaries. This intepretation is guided by results obtained in the present work by simulation of grain boundaries using finite-element techniques of numerical analysis. In the course of the experimental investigations, we have also discovered that, in the Wacker material at least, the grain-boundary potential cannot generally be regarded as uniform over the grain-boundary plane. Several other observations of a presently qualitative nature indicate that the carrier transport at grain boundaries can be a rather complex process.

II. THE GRAIN-BOUNDARY INTERFACE

The grain boundary in a polycrystalline semiconductor is an interface between two identical crystals of different orientation. The mismatch in bonding between the two crystals results in bond defects (e.g., distorted bond angles, dilated or compressed bonds, broken bonds) at the grain boundary. These defects are expected to exist primarily on a single plane of atoms, and to a lesser extent on the neighboring planes. We consider the width of the grain-boundary region to be negligible on the scale of variations in the potential in the adjacent space-charge regions.

The bonding defects at the grain boundary translate into localized electronic states or interface states. The energy distribution of these states is of importance in the determination of carrier-transport processes. There is in general a net charge associated with the grain-boundary interface states, which is modified by a voltage applied across

the grain boundary. The interface states also function as recombination centers for excess electrons and holes at the grain boundary. It has been observed that for grain boundaries in n-type silicon, the interface states inevitably contribute a net negative charge.[6] In p-type silicon the grain-boundary interface states contribute a positive charge.[6] The reason for this difference in n- and p-type silicon is the difference in the position of the Fermi energy relative to the interface-state distribution in the two cases.

In order to be specific we restrict our discussion to the case of grain boundaries in p-type silicon. This is the case which pertains to the experimental work reported below, and to the energy-band diagram of Fig. 1. It is assumed that positive charge associated with the interface states is balanced by a net negative charge due to uncompensated ionized acceptor impurities. These acceptor impurities are located in space-charge regions adjacent to the grain boundary in the crystalline regions to either side. It is assumed that the interface charge is uniformly distributed over the area of the grain boundary. The magnitude of the potential barrier at the grain boundary for zero applied bias voltage (V_{d0} in Fig. 1) is referred to as the diffusion potential of the grain boundary.

Poisson's equation relates the charge distribution to the electrostatic potential. This may be expressed as

$$\nabla^2\phi_i = -\frac{\rho}{\epsilon} , \tag{1}$$

where ϕ_i is the electrostatic potential, ϵ is the permittivity of the semiconductor, and ρ is the charge density given by

$$\rho = q(p - n + N_d^+ - N_a^-) + Q_{is} . \tag{2}$$

In Eq. (2), Q_{is} is the net charge in the grain-boundary interface states and N_d^+, N_a^- are the ionized donor,acceptor impurity concentrations in the semiconductor (assumed uniformly distributed in space). For the p-type material discussed in this paper, $N_d = 0$ in Eq. (2). In general Q_{is} is a function of n and p, the concentrations of electrons and holes, at the grain boundary. These carrier concentrations are given by

$$n = n_i \exp\left[\frac{E_{Fn} - E_i}{kT}\right] , \tag{3}$$

$$p = n_i \exp\left[\frac{E_i - E_{Fp}}{kT}\right] , \tag{4}$$

where E_{Fn}, E_{Fp} are the quasi-Fermi-levels for electrons and holes, respectively. In Eq. (1) the potential ϕ_i may be replaced by $-E_i/q$ where the energy E_i, which appears in (3) and (4), is known as the intrinsic level (see Fig. 1). The charge Q_{is} in grain-boundary interface states is dependent upon the energy distribution of these states, and also upon their charge state when occupied by an electron (donorlike or acceptorlike).

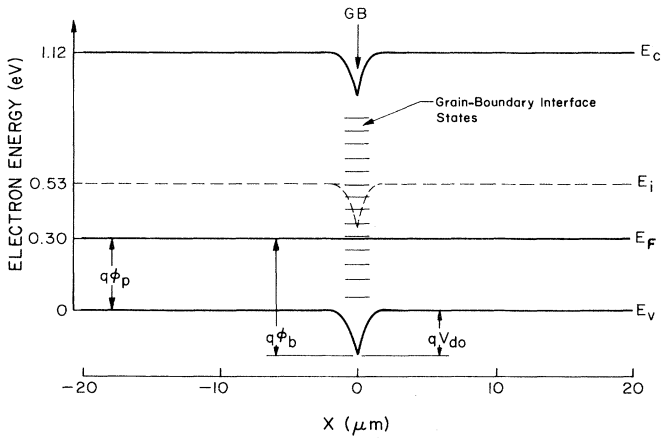

FIG. 1. Numerical calculations of electron energy-band diagram of the grain boundary under equilibrium conditions ($V=0$, dark), showing the diffusion potential V_{d0}, barrier height ϕ_b, bulk Fermi potential ϕ_p, intrinsic energy level E_i, and interface states present at $X=0$; $N_a = 10^{20}\ \mathrm{m}^{-3}$, $T = 300$ K, and $Q_{is} = 1.5\times10^{14} q\ \mathrm{C\,m}^{-2}$.

III. CARRIER TRANSPORT ACROSS GRAIN BOUNDARIES

In the preceding section, we have described the processes which contribute to the formation of a diffusion potential, or potential barrier against the transport of majority carriers across grain boundaries in semiconductors such as silicon. We have also introduced the localized interface states, which act as recombination centers for electrons and holes, and which modify the diffusion potential by adjusting their charge according to the concentrations of electrons and holes at the grain boundary. In this section we address the major theme of this work: electron and hole transport processes.

In order to model the transport of electrons and holes analytically, an appropriate transport model must be adopted. To guide this procedure, we have performed a simulation of grain-boundary transport using finite-element methods of numerical analysis, which employ the Newton-Raphson algorithm (Appendix A).

To simplify the interpretation of these numerical results, we have solved for the case where the charge in grain-boundary interface states Q_{is} is fixed, and does not depend on bias voltage applied across the boundary. In addition, we ignore recombination through grain-boundary interface states. While it is realized that these assumptions are unphysical in a real grain boundary, they provide for the analysis of electron and hole transport uncomplicated by the effects of recombination at this interface.

An example of the results of the numerical calculations is given in Fig. 2, which shows the dependence of the electron and hole quasi-Fermi-potentials, and of the electrostatic potential, upon position for a voltage V applied across the grain boundary. Note that in this figure, as well as Fig. 3, the quasi-Fermi-level $E_{Fn} \neq E_{Fp}$ as a consequence of dark generation-recombination currents.[17] The effect of this voltage is to lower the potential barrier, or band bending, on the forward-biased side of the boundary and to increase it on the opposite (reverse-biased) side. The voltage division between these two sides depends, among other things, upon the charge in grain-boundary interface states, Q_{is}, and in particular on the manner in

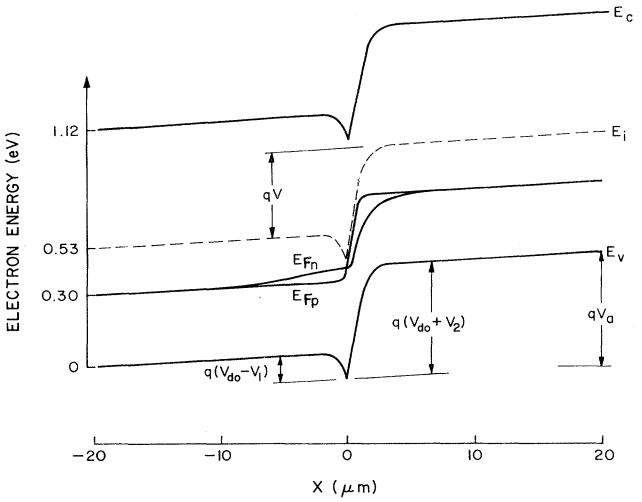

FIG. 2. Numerical calculations of electron energy-band diagram under applied bias voltage V, showing quasi-Fermi-levels E_{Fn} and E_{Fp} for electrons and holes, and voltage division V_1 and V_2 between forward-biased and reversed-biased space-charge regions. (Note: $V=V_1+V_2$.) V_a is the total applied voltage from $X=-20$ to $+20$ μm, which is approximately equal to V except at very large current densities. Slope of energy bands and potentials away from grain boundaries is associated with voltage drop in the series resistance of the grains. This contributes to V_a. $\tau=(\sigma v_{\rm th}N_t)^{-1}=10^{-9}$ s, $N_a=10^{20}$ m^{-3}, $T=300$ K, and $Q_{is}=1.5\times10^{14}q$ C m^{-2}.

which this charge changes under applied bias voltage. However, in the calculation of Fig. 2, the effects of changing Q_{is} are not considered, as discussed above.

We consider the mechanism by which holes cross the grain boundary in similar generality to the earlier treatment of the metal-semiconductor contacts, or Schottky barriers.[7] The holes must negotiate the space-charge region by the usual drift and diffusion mechanisms and upon arriving at the grain boundary either be accepted into the other side, or be reflected. The opposite side of the grain boundary is the same semiconductor, but with a different crystal orientation. The acceptance of the holes can be regarded as a process of interface emission characterized by a collection velocity v_r, which is in series with the drift and diffusion processes.

In the Schottky barrier, at least for high-mobility semiconductors such as silicon, the thermionic emission of the majority carriers (holes) into the metal becomes the bottleneck to current flow. This has been discussed by Gossick,[8] and more recently by Rhoderick.[9] The reason is that there are very few available states in the metal with momentum parallel to the surface to match that of the holes from the semiconductor. This is because the energy at which the holes are transferred is close to the valence-band edge in the semiconductor, but remote from the band edges in the metal.

In the present problem, however, the states on either side of the grain boundary have the same energy relative to the band edges. The limitations due to conservation of parallel momentum are greatly relaxed. We also deal with diffusion potentials which are much smaller than those normally encountered in Schottky barriers. In addition there exists, on the reverse-biased side, a large electric field which is attractive to the majority carriers. The consequence of these factors is that holes, upon reaching the grain-boundary interface, are collected efficiently and the supply of these carriers through the space-charge region may become the limiting factor in determining the current. Following the work of Rhoderick[9] and of Crowell and Sze,[7] we consider the energy diagram of Fig. 3 and the extremes of hole concentration at the grain boundary when transport is limited by diffusion (case 1, curve D) or by emission (case 2, curve E).

We suggest that a general approximate expression for the intermediate case may, on the basis of Refs. 7 and 3, be written

$$J_p=\frac{qN_v v_r}{1+\dfrac{v_r}{v_d}}\exp\left[-\frac{\phi_b}{V_T}\right]\left[\exp\left[\frac{V_1}{V_T}\right]-\exp\left[-\frac{V_2}{V_T}\right]\right]$$
$$=\frac{qN_v N_r}{1+\dfrac{v_r}{v_d}}\exp\left[-\frac{\phi_b}{V_T}\right]\exp\left[\frac{V_1}{V_T}\right]\left[1-\exp\left[-\frac{V}{V_T}\right]\right], \quad (5)$$

since $V=V_1+V_2$, where V is the total voltage applied across the grain boundary, V_1 is the forward bias on the left side of the grain boundary in Fig. 2 which is so far an undetermined portion of V and V_2 is the reverse bias on the right side of the boundary. v_d and v_r are the diffusion and interface recombination (or in our case collection) velocities for the holes, respectively. ϕ_b is the equilibrium barrier height which is independent of V (Fig. 1); N_v is the effective density of states in the valence band; $v_d=\mu\xi_{m1}$ with ξ_{m1} the maximum electric field in the space-charge region on the forward-biased side of the grain boundary.

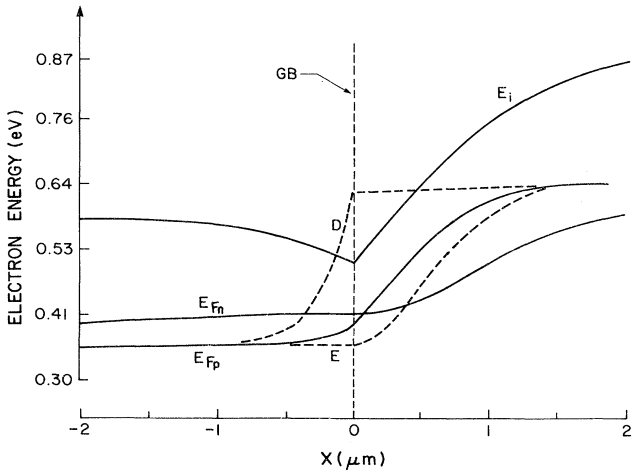

FIG. 3. Expanded view of calculations in neighborhood of the grain boundary (GB) for the case of Fig. 2. Curves D and E show schematically the limiting cases of diffusion- and emission-limited transport.

In the present case $v_r = \mu \xi_{m2}$, with ξ_{m2} the maximum field on the reverse-biased side. For any appreciable voltage across the boundary, $\xi_{m2} \gg \xi_{m1}$ and $v_r \gg v_d$ in Eq. (5).

In case 1 (shown schematically as D in Fig. 3), the interface collection velocity v_r is considered to be large. The hole current is then limited by diffusion through the (forward-biased) space-charge region and the concentration of holes at the grain boundary remains small under applied voltage. This is illustrated by a rise in the hole quasi-Fermi-level E_{Fp} as the grain boundary is approached from the forward-biased side. The transfer of holes across the grain boundary which in this case is proportional to their concentration at $x=0$, $p(0)$ is kept small by the limited supply to the boundary. On the other hand, if the collection velocity v_r is small (case 2 and E in Fig. 3) holes arriving at the grain boundary are not immediately removed by the reverse-biased side. The supply of holes to the grain boundary is bountiful and $p(0)$ increases to its maximum value determined by the hole Fermi level on the forward-biased side. In this case E_{Fp} is relatively flat up to the grain boundary. As we observe in Figs. 2 and 3 which show the results of an exact calculation, the true situation is intermediate between these extremes, with E_{Fp} rising (in this case by more than kT) as the grain boundary is approached.

On the basis of the results of Figs. 2 and 3 from the numerical analysis, we believe that the diffusion model ($v_r \gg v_d$), as originally described by Stratton,[10] is the appropriate basis for the interpretation of majority-carrier transport across grain boundaries. This model is employed in the analysis of the experimental data of the following sections.

IV. SAMPLE FABRICATION AND MEASUREMENTS

The material used in this study was p-type cast silicon of large grain size (typically 1 mm) of the "Silso" type, obtained from Wacker Chemitronic Ltd. The doping concentration N_a from bulk measurements (e.g., C^{-2} vs V of Schottky-barrier capacitance-voltage characteristics for diodes within single grains) was $\simeq 3 \times 10^{21}$ m^{-3}. The polycrystalline wafers ($100 \times 100 \times 0.4$ mm^3) were cut into strips approximately 1×20 mm. These strips were chemically polished in 3:1:1 HNO_3 (79%), HF (49%), glacial acetic acid, for $\simeq 3$ min to eliminate saw damage and to highlight the grain boundaries.[11] Grain boundaries were examined under an optical microscope to identify those which were planar and which extended over the entire cross section of the strip in both the lateral and vertical directions; the latter requirement was determined by examining the back face of the samples.

Aluminum contacts were evaporated in a four-probe configuration (Fig. 4) and were sintered at 600 °C for 2 min in N_2 to form Ohmic contacts. Aluminum connections were bonded to the (inner two) voltage-measurement contacts. A single grain boundary was then enclosed between the voltage probes. Current was injected and removed at the outer two contacts. Contact potential errors in the determination of the voltage across the grain boundary were avoided by means of this four-probe technique; voltages were measured using a Keithley 610C electrometer with input impedance of 10^{11} Ω. All measurements were made under dc conditions.

Measurements at temperatures from 300 to 200 K were performed in a FTS Systems Inc. Multi-Cool closed-cycle refrigeration unit. For temperatures from 100 to 200 K a cryogenic liquid-nitrogen sample chamber fitted with a

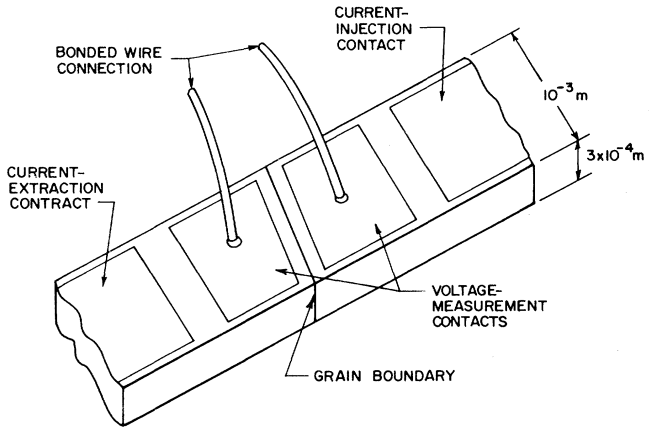

FIG. 4. Sample geometry. Cross-sectional area of all samples $\simeq 3 \times 10^{-7}$ m^{-2}.

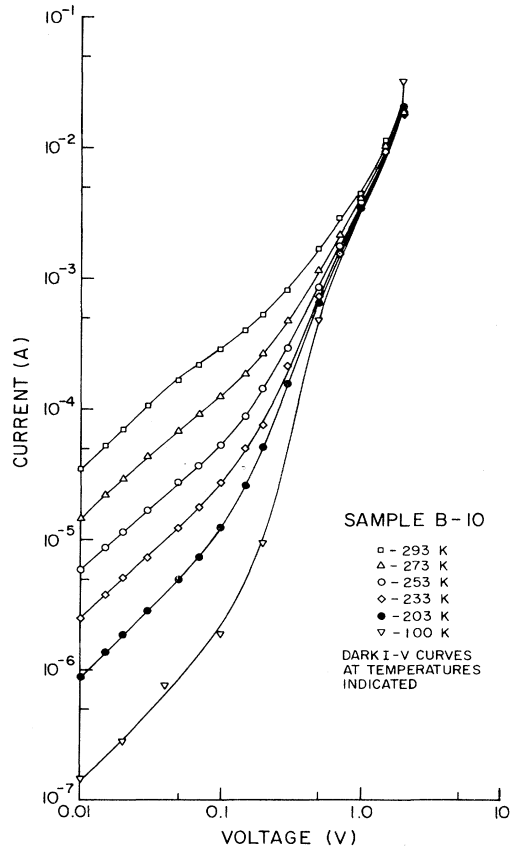

FIG. 5. Experimental dark characteristics of grain boundary B-10 at several measurement temperatures.

heater for temperature variation was employed. Temperatures were measured using Cu-Co thermocouples. Optical illumination was provided by a Sylvania ELH projection lamp with an infrared filter to remove all photon wavelengths $\lambda < 1\ \mu m$. This ensured a relatively uniform photogeneration throughout the sample. The optical intensity was determined using an Optikon Model 550-1 radiometer. The accuracy of this determination was approximately $\pm 30\%$. The reflection from the silicon surface was estimated to be 30%.

The equilibrium grain-boundary diffusion potential, V_{d0}, was observed to vary over a wide range for samples cut from different grain boundaries [V_{d0} values from < 0.1 V (electrically inactive) to $\simeq 0.33$ V at 300 K].

V. EXPERIMENTAL RESULTS

Figure 5 shows a typical example of the current-voltage characteristics measured on a grain boundary having a relatively large zero-bias diffusion potential ($V_{d0} \simeq = 0.25$ V at 300 K). Results are given for a number of measurement temperatures. Measurements such as these were performed for a variety of samples over the temperature range $100 \leq T \leq 300$ K. Figure 6 shows a typical example of the corresponding characteristics for a grain boundary with a somewhat smaller (zero-bias) diffusion potential. These grain boundaries turn out to exhibit a spatial variation in their properties over the boundary plane. Figure 7 is representative of a different case of grain boundary in which the potential barrier is spatially uniform, as we discuss in a later section.

The effect of optical illumination on the grain-boundary current-voltage characteristics is illustrated in Figs. 8 and 9. This data was obtained for optical powers of 0.2 and 50 $W m^{-2}$, respectively, with $1.0 \leq \lambda \leq 1.1\ \mu m$. A range of optical-illumination intensities was investigated, but the rather complicated behavior observed at higher intensities is still under study at this time.

In Fig. 10 we show the dependence of the activation energy E_a (defined in Sec. VI) upon the voltage V applied across a boundary region. This activation energy is determined from the temperature dependence of the current-voltage characteristics such as those of Figs. 5—7. Figure 11(a) shows the dependence of E_a upon T (determined at a low value of V) for two of the same samples. From Fig. 11(a) and the expressions of Sec. III we are able to derive the equilibrium (dark, zero-bias) diffusion potential V_{d0}, assuming that this potential is spatially uniform over the boundary plane. This is shown in Fig. 11(b), together with the result expected from a one-dimensional theory. Figures 12(a) and 12(b) give the observed dependence of E_a and V_d upon optical illumination intensity (at 300 K) for the same samples. In this case V_d is no longer the *equilibrium* diffusion potential V_{d0}.

It was also observed that for large grain-boundary voltages, and hence moderately large current densities ($\simeq$10—50 V and $4\times10^5 - 1\times10^6$ $A m^{-2}$), the current exhibited oscillations such as those shown in Fig. 13.

The magnitude of these oscillations was typically on the order of 1% of the dc current. It was observed that a sample biased below the threshold current density for these oscillations could be thermally stimulated into oscillation. Generally, more and larger pulses are observed at higher current densities, and these effects are reversible. We believe these oscillations are due to field emission of carriers from grain-boundary interface states, as discussed in a later section.

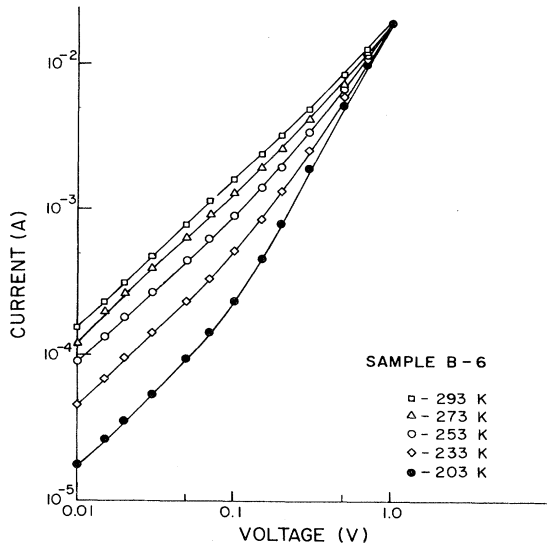

FIG. 6. Experimental dark characteristics of grain boundary B-6 at several measurement temperatures.

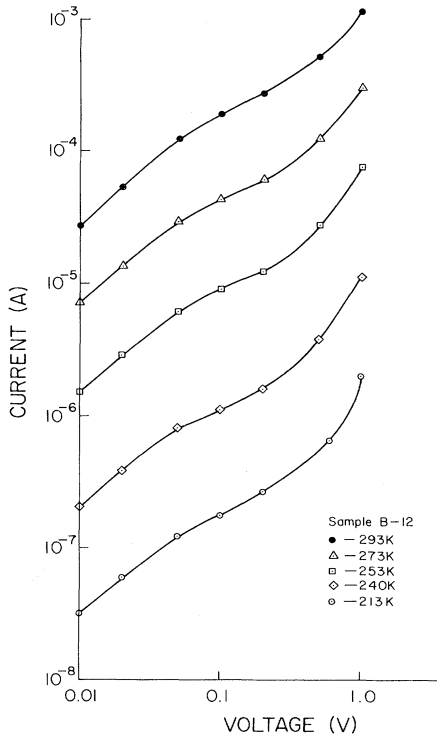

FIG. 7. Experimental dark characteristics of grain boundary B-12 at several measurement temperatures.

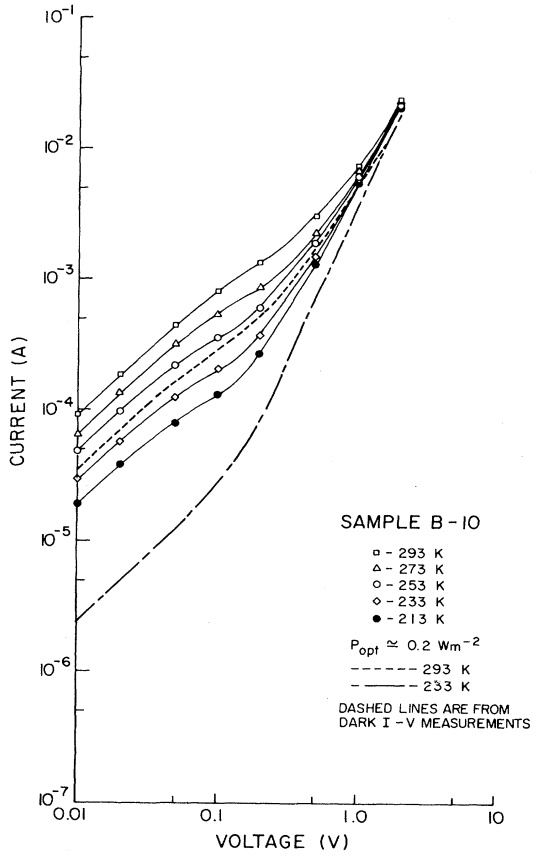

FIG. 8. Experimental characteristics of B-10 under 0.2 W m^{-2} optical illumination ($1.0 < \lambda < 1.1$ μm).

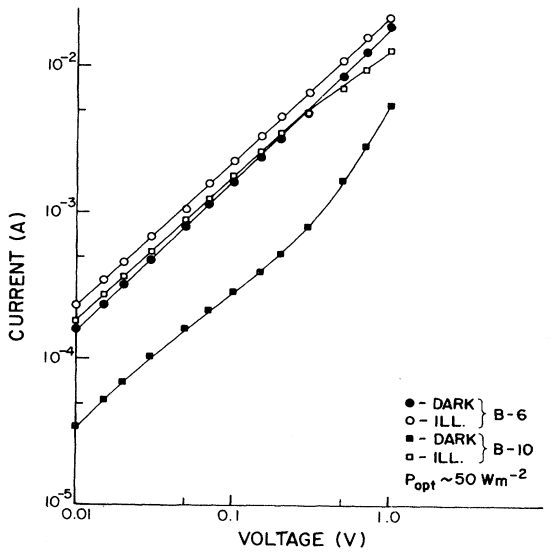

FIG. 9. Experimental characteristics of B-6 and B-10 under 50 W m^{-2} ($1.0 < \lambda < 1.1$ μm) optical illumination.

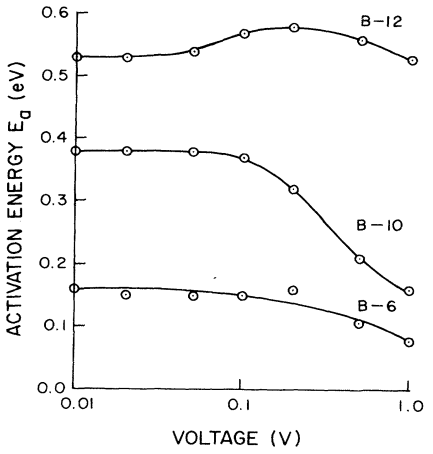

FIG. 10. Activation energy E_a vs V applied to grain boundaries B-10, B-6, and B-12.

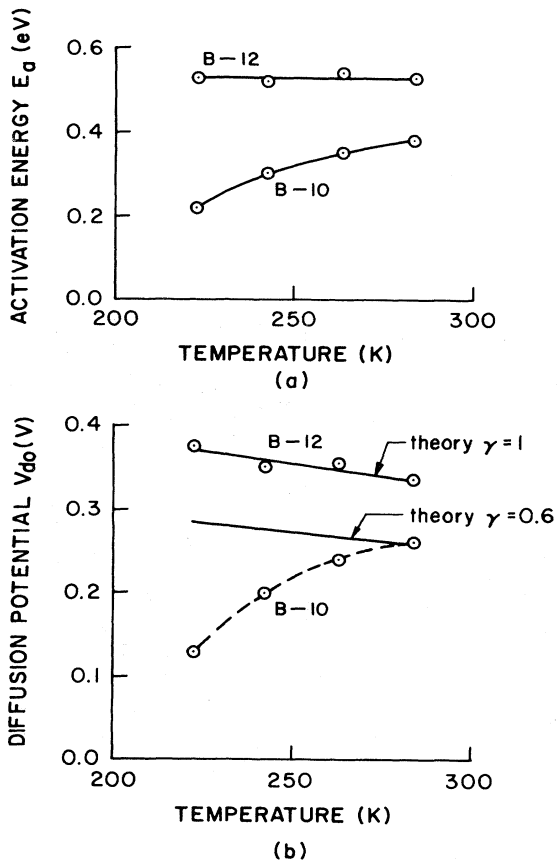

FIG. 11. Dependence of (a) the activation energy and (b) the diffusion potential on temperature for B-10 and B-12 in darkness.

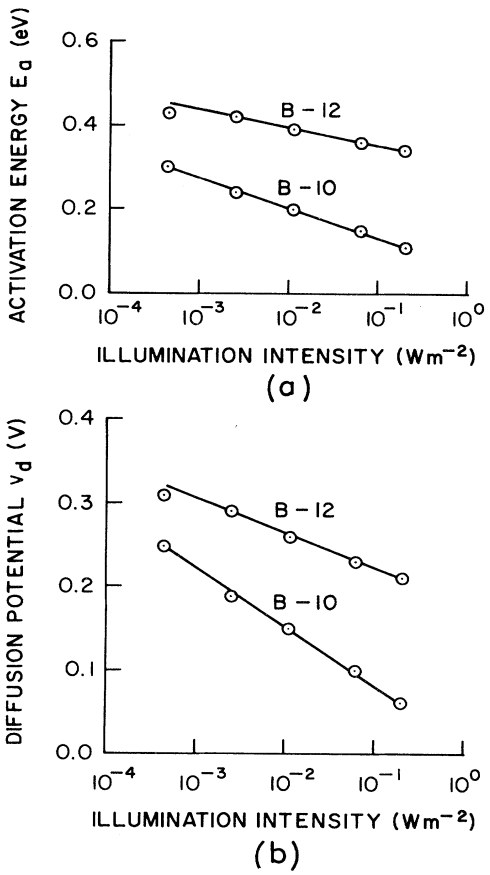

FIG. 12. The dependence of (a) the activation energy and (b) the diffusion potential on illumination intensity for B-10 and B-12. $T=300$ K.

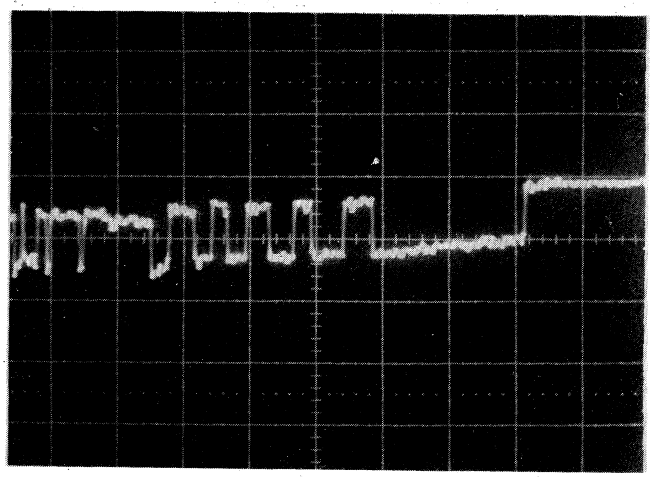

FIG. 13. Current oscillations observed at high dc current densities. Grain-boundary sample B-11. $V=15$ V; $I=150$ mA. Vertical scale: 500 μA/division. Horizontal scale: 1 ms/division.

VI. INTERPRETATION OF RESULTS

The steady-state current-voltage characteristics of the grain boundary in general consist of a component due to the transport of majority carriers over the grain-boundary potential barrier, J_1, a component due to minority carriers transported in the opposite direction, J_2, and finally a component associated with recombination of electrons and holes in grain-boundary interface states, J_3. These three components are illustrated in the energy-band diagram of Fig. 14. Our interpretation of results from the preceding section is that the first component is completely dominant over the other two, at least under dark conditions. That is, currents such as those of Figs. 5—7 are to be identified with the transport of majority carriers (in our case, holes) over the potential barrier at the grain boundary. (The downward bending of the bands at the grain boundary presents a barrier to holes.) In this interpretation we are in agreement with previous workers.[2–4,12–15] We do, however, consider the other two components in their *indirect* effects upon the majority-carrier current. This will be discussed further below.

In view of the discussion of Sec. III, we adopt the diffusion-limited value of Eq. (5) for the majority-carrier current J_1. In this case ($v_r \gg v_d$), Eq. (5) becomes

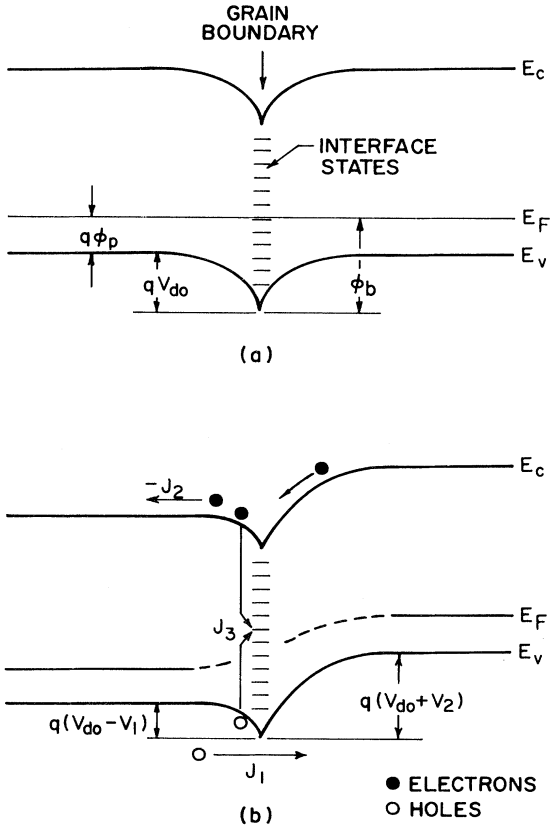

FIG. 14. Electron energy-band diagrams for grain boundary with (zero-bias) diffusion potential V_{d0}. (a) $V=0$; (b) $V>0$. J_1 is the majority-carrier current, J_2 is the minority-carrier current, and J_3 is the recombination current at the grain boundary.

$$J \simeq J_1 \simeq qN_v v_d \exp\left[-\frac{\phi_b}{V_T}\right]\exp\left[\frac{V_1}{V_T}\right]\left[1-\exp\left[-\frac{V}{V_T}\right]\right]$$
$$= qN_v \mu \xi_{m1} \exp\left[-\frac{\phi_p}{V_T}\right]\exp\left[-\frac{V_{d0}}{V_T}\right]\exp\left[\frac{V_1}{V_T}\right]\left[1-\exp\left[-\frac{V}{V_T}\right]\right]$$
$$= qN_a \mu \xi_{m1} \exp\left[-\frac{V_{d0}}{V_T}\right]\exp\left[\frac{V_1}{V_T}\right]\left[1-\exp\left[-\frac{V}{V_T}\right]\right], \quad (6)$$

where $\phi_b = V_{d0} + \phi_p$ (Fig. 14) and we have used $\exp(-\phi_p/V_T) \simeq N_a/N_v$ which is true provided the acceptor impurities (of concentration N_a) remain ionized, i.e., for $T \geq 100$ K in silicon.

For $V \ll V_T$ and $V_1 \ll V_T$ we can simplify (2) to

$$J \simeq qN_a \mu \xi_{m1} \left[\frac{V}{V_T}\right]\exp\left[-\frac{V_{d0}}{V_T}\right], \quad (7)$$

and define an activation energy for the potential barrier at the grain boundary as

$$E_a = -\frac{d \ln\left[\dfrac{J}{qN_a \mu \xi_{m1}(V/V_T)}\right]}{d(1/kT)}$$
$$= qV_{d0} + q\frac{d(V_{d0})}{d(1/T)}$$
$$= q\left[V_{d0}(T) - T\frac{dV_{d0}}{dT}\right]. \quad (8)$$

Equations (7) and (8) apply for $V \ll V_T$. For relatively large applied voltages, on the other hand, i.e., for $V \gg V_T$, they are replaced by

$$J \simeq qN_a \mu \xi_{m1} \exp\left[-\frac{V_{d0}}{V_T}\right]\exp\left[\frac{V_1}{V_T}\right]$$
$$= qN_a \mu \xi_{m1} \exp\left[-\frac{V_d}{V_T}\right], \quad (7')$$

where $V_d = V_{d0} - V_1$, and

$$E_a = -\frac{d \ln\left[\dfrac{J}{qN_a \mu \xi_{m1}}\right]}{d(1/kT)}$$
$$= q(V_{d0} - V_1) + \frac{q}{T}\frac{d(V_{d0} - V_1)}{d(1/T)}$$
$$= q\left[V_d(T) - T\frac{dV_d}{dT}\right]. \quad (8')$$

Note that the second term on the right-hand sides of Eqs. (8) and (8') turns out to be negative, as discussed below and exactly cancel the temperature dependence of the first term *for spatially uniform grain boundaries,* so that in this case $E_a \neq E_a(T)$.

We have chosen to take the temperature dependence of the low-field mobility given by[16]

$$\mu(T) = 54.3T_n^{-0.57} + \frac{1.36\times10^8 T^{-2.23}}{1+[N_a/(2.35\times10^{17}T_n^{2.4})]0.88T_n^{-0.146}} \quad (9)$$

($T_n = T/300$) to the left-hand side in Eqs. (8) and (8'). In these equations, the parameters J, μ, and V_{d0} are temperature dependent, in addition to the explicit appearance of T and $V_T = kT/q$.

The equilibrium diffusion potential V_{d0} in Eq. (8) is temperature dependent for two reasons. First, the temperature dependence of the bulk Fermi potential ϕ_p, given by

$$\phi_p = \frac{kT}{q}\ln(N_v/N_a), \quad (10)$$

gives rise to a temperature dependence of V_{d0} which may be written as

$$\frac{dV_{d0}}{dT} = -\gamma\frac{d\phi_p}{dT} \simeq -\frac{\gamma k}{q}\ln\left[\frac{N_v}{N_a}\right], \quad (11)$$

where we have used Eq. (10) and neglected the weak temperature dependence of $\ln N_v$. γ is a parameter which accounts for Fermi-level pinning at the grain boundary by interface states. For samples B-12 and B-10, for example, we have that $\gamma \simeq 0.9$–1.0 and $\gamma \simeq 0.6$, respectively, for the N_{is} measured in these samples (see Appendix B for derivation of γ).

Second, the occurrence of a spatial variation of diffusion potential over the grain-boundary plane will give rise to an "effective V_{d0}" in Eq. (7) which also exhibits a temperature dependence in addition to that of Eq. (11). This is because the current transport through various portions of the grain boundary with different V_{d0} will be weighted by the temperature-dependent factor $\exp(-qV_{d0}/kT)$. At lower temperatures a larger portion of the current will flow through the regions of lowest V_{d0} and the effective V_{d0} will decrease. For a spatially uniform grain boundary dV_{d0}/dT is therefore given by Eq. (11), whereas for a nonuniform boundary, an additional term dependent upon the nature of the spatial nonuniformity contributes to dV_{d0}/dT.

The maximum electric field ξ_{m1} in Eq. (7) corresponds to that close to the grain boundary on the left-hand side of Fig. 14, given in the depletion approximation by[17]

$$\xi_{m1} \simeq \left[\frac{2qN_a}{\epsilon_s} (V_{d0} - V_1 - V_T) \right]^{1/2} , \tag{12}$$

where ϵ_s is the silicon permittivity.

As the applied voltage V increases, we have that

$$V = V_1 + V_2 , \tag{13}$$

$$Q_1 = -qN_a W_1 = -[2q\epsilon_s N_a (V_{d0} - V_1 - V_T)]^{1/2} , \tag{14}$$

$$Q_2 = -qN_a W_2 = -[2q\epsilon_s N_a (V_{d0} + V_2 - V_T)]^{1/2} , \tag{15}$$

and

$$Q_1 + Q_2 + Q_{is} = 0 \tag{16}$$

for all V. V_{d0}, V_1, and V_2 have been defined above; W_1 and W_2 are the widths of the space-charge regions on the forward- and reverse-biased sides of the grain boundary, respectively. Q_1 and Q_2 are the charge (per unit area) in these space-charge regions (within the depletion approximation), and Q_{is} is the charge per unit area in the grain-boundary interface states.

Let us assume that the grain-boundary interface states remain in equilibrium with the majority carriers (holes) under an applied bias voltage. If we adopt the convention of earlier workers[3,4] that the *change* with bias voltage in the quasi-Fermi-level at the grain-boundary interface is approximately equal to the change of its value in the bulk on the forward-biased side, it then follows that

$$Q_{is}(V) = Q_{is}(0) + qN_{is} V_1 \tag{17}$$

for an interface-state density $N_{is}(\mathrm{m}^{-2}\mathrm{eV}^{-1})$ which is independent of energy. For an energy-dependent interface-state density, $N_{is} V_1$ in Eq. (17) must be replaced by $\int N_{is} dV_1$.

It is important to realize that the value of N_{is} deduced from measurements using Eq. (17) represents a *lower limit* on the true interface-state density. From our discussion of the majority-carrier transport above, we anticipate a hole transport which is restricted by the supply of holes to the grain boundary (diffusion model) and an appreciable change in the hole quasi-Fermi-level E_{Fp} across the forward-biased space-charge region. Thus the change in E_{Fp} at the grain boundary with applied voltage may be somewhat less than V_1 and N_{is} will be underestimated using Eq. (17) with the experimentally-determined $Q_{is}(V)$.

Finally, we point out that the grain boundaries were modeled as planar interfaces; the possibility of curvature on a macroscopic scale was not accounted for. This may affect the numerical values of N_{is} to some degree.

VII. DISCUSSION OF RESULTS

We have used the diffusion model of Sec. III to analyze the results of Figs. 5—12. This treatment assumes a grain-boundary potential which is spatially uniform over the boundary plane, in accordance with the one-dimensional analysis.

As a general interpretation of the current-voltage characteristics of Figs. 5—7, at very low voltages ($V < V_T$) the curves are near Ohmic as expected from Eq. (7). At higher voltages, the increase in J with V originates primarily from the $\exp(V_1/V_T)$ term in Eq. (6). The detailed shape of the characteristic depends upon the variation of V_1 with V, which in turn is controlled by the degree of pinning of the quasi-Fermi-level for holes by grain-boundary interface states. The concave nature of these curves at higher V is associated with a high density of interface states N_{is} near midgap (strong pinning), which drops off appreciably towards the valence band. This interpretation is consistent with that offered by Seager *et al.*[2-4] for grain boundaries in n-type silicon, in which case N_{is} also falls towards the conduction band.

N_{is} is an important parameter since, among other things, this determines the appropriate value of γ to be used in Eq. (11). We have determined N_{is} as a function of energy by analysis of the current-voltage characteristics at a constant temperature (Fig. 5) in terms of the diffusion theory of the carrier transport. This is in the spirit of the deconvolution scheme of Seager *et al.*,[2-4] and data at three measurement temperatures have been combined to give rise to the N_{is} vs E of Fig. 15. For this sample γ is then determined to be 0.6, as described in the Appendix. Our results for N_{is} agree within an order of magnitude with those obtained by Seager *et al.*,[2-4] in their case in the upper half of the band gap in neutron-transmutation-doped silicon. Comparison of $N_{is}(E)$ with earlier workers is made in Fig. 16. The picture which emerges is a peak in the density of interface states of magnitude $N_{is} \simeq 10^{16}$ $\mathrm{m}^{-2}\mathrm{eV}^{-1}$ or greater at the peak and of energy spread $\Delta E \simeq 0.1$ eV.

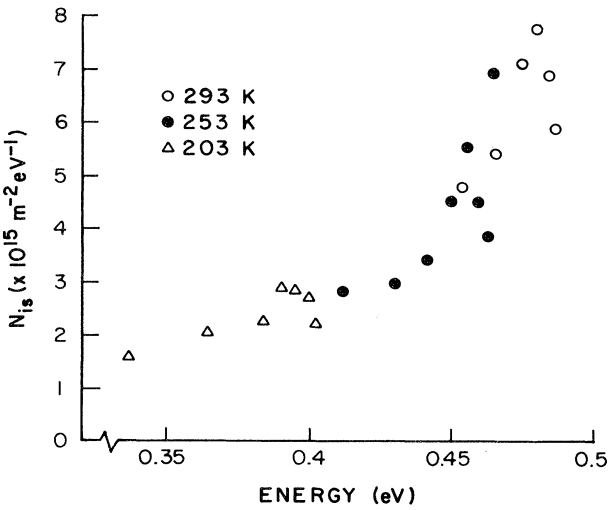

FIG. 15. Density of localized grain-boundary interface states vs energy in band gap of silicon (sample B-10). Points show results obtained from current-voltage characteristics at constant temperature T, for three values of T.

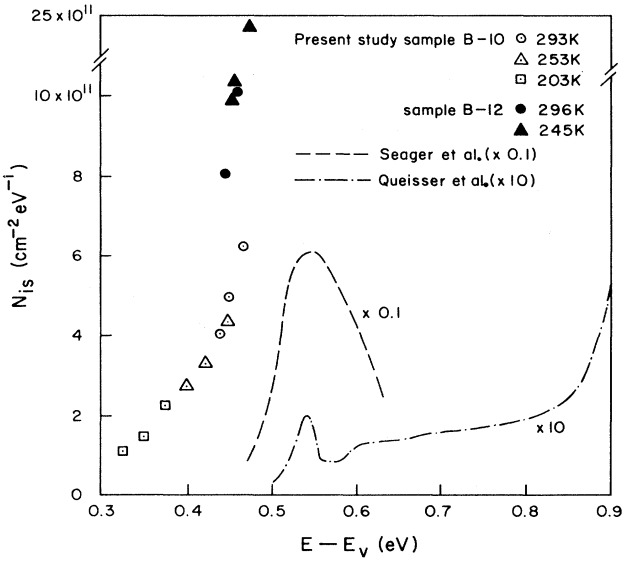

FIG. 16. Comparison of present results for grain-boundary interface states with earlier results for silicon grain boundaries (Refs. 27 and 28). Note units of N_{is} are $\mathrm{cm}^{-2}\mathrm{eV}^{-1}$ for this figure.

In Fig. 10 we show the dependence of the activation energy E_a (defined in Sec. VI) upon the voltage applied to the grain boundary. In the determination of E_a, the temperature dependence of the mobility, given by Eq. (9), has been removed, i.e., $\ln[J/qN_a\mu(T)\xi_{m1}]$ is plotted versus $1/T$, and the slope used to find E_a in accordance with Eq. (8′). For grain boundaries which are spatially uniform, we can interpret the decrease in E_a at the larger V unambiguously as arising from a decrease in diffusion potential $V_d = V_{d0} - V_1$ due to the increase in V_1 [see Eq. (8′)]. As we see below this is the case for grain-boundary sample B-12 but not for B-10 or B-6.

One should realize that the considerably smaller value of E_a for sample B-6 as compared to B-10 and B-12 is a property of the temperature dependence of the current. This does not imply that the absolute value of the current density at a given temperature is much larger. The value of the current density is controlled by the diffusion potential V_{d0}, which for sample B-6 is not significantly lower than for the other samples. The relation between V_{d0} and E_a is strongly dependent on the nonuniformity of the grain boundary.

The increase in E_a with V at low voltages for B-12 in Fig. 10 arises from the preexponential factor in Eq. (6). The temperature dependence of the low-field mobility has been accounted for in arriving at E_a. The temperature dependence of the high-field mobility is smaller than that of the low-field mobility since we are approaching the region of velocity saturation.[17] Since the electric field ξ_{m1} decreases with V, the activation energy at larger V therefore increases.

In the case of grain boundaries B-6 and B-10, arguments which follow indicate that these samples exhibit substantial nonuniformity in their diffusion potentials over the plane of the grain boundary. This prohibits the analysis of the results of Fig. 10 for B-6 and B-10 in terms of the model of Sec. VI, which presupposes spatially uniform grain-boundary potentials.

In Fig. 11 we show how E_a and V_{d0} depend upon temperature for the two grain boundaries B-10 and B-12. For a uniform grain boundary, the activation energy E_a will correspond to V_{d0} for very small N_{is} ($\gamma=0$) and to ϕ_b in Fig. 14 for very large N_{is} ($\gamma\simeq 1$). It must be stressed that, in order to recover the equilibrium diffusion potential V_{d0} from the activation energy E_a, we must employ the analysis of Sec. VI and in particular Eq. (8), since $V < V_T$ in the experimental determination of E_a. Knowing the γ to be used in Eq. (11), we obtain dV_{d0}/dT for Eq. (8) which allows us to determine V_{d0} from E_a. We have therefore implicitly assumed grain boundaries which are *spatially uniform* in their properties. In Fig. 11(b) we show the results of this procedure for B-10 and B-12, together with the dependence of V_{d0} upon T expected theoretically. As we readily observe, B-12 conforms well to the uniform model of Sec. VI with a V_{d0} which decreases slightly with T, in accordance with the temperature dependence of the bulk Fermi potential ϕ_p.

On the other hand, as was discussed in the paragraph following Eq. (11), a grain boundary with spatially nonuniform properties may show a marked *increase* of E_a and V_{d0} with T. This is the case for sample B-10 in Fig. 11. We conclude that while B-12 represents a uniform grain boundary which is suitable for the model of Sec. VI, and which therefore allows an accurate quantitative determination of $V_{d0}(T)$ as in Fig. 11(b), sample B-10 does not. The data of Fig. 11(b) are not expected to be quantitatively correct for B-10, and the most we can say is qualitatively that the apparent V_{d0} increases substantially with increasing temperature as a consequence of its spatially nonuniform grain-boundary potential. Even if Eq. (7) applies with an "effective" $V_{d0}(T)$, the unknown form of the temperature dependence excludes a separation of the two terms on the right-hand side of Eq. (8) for nonuniform samples. We have separately obtained a first-order model for B-10 by assuming a Gaussian distribution of V_{d0} values over the grain-boundary plane.[18] The errors are rather large in this fitting procedure, presumably because a Gaussian distribution of potentials is unphysical in this problem.

The origin of the nonuniformity in diffusion potential for B-10 (also B-6 and others, not shown) is thought to be a spatial variation over the plane of the grain boundary in N_{is}, in N_a, or both. This nonuniformity must be over macroscopic distances (greater than the width W_1, W_2 of the space-charge regions) since otherwise their effects would be integrated electrostatically. The segregation of dopant impurities to the grain boundary can also affect the interface-state distribution in a spatially nonuniform way. We are presently working to quantity this model, which gives a three-dimensional nature to the transport problem. We must point out that in the work of Seager *et al.*,[2–5] the impurities were introduced by neutron-transmutation doping, which is expected to produce a uniform N_a, unlike the present case of cast silicon with dopant introduced into the melt.[19] At any rate, it seems

fairly certain that both uniform and nonuniform grain boundaries exist in the Wacker silicon material of this study.

One possible source of spatial nonuniformity is the surface region of the sample. We are satisfied that this is not important in our samples on the basis of experiments with a zerostat, which allows us to deposit either positive or negative charge on the surface.[20] The deposition of negative charge causes a noticeable temporary increase in the current across the grain boundary, undoubtedly because the potential barrier of this boundary is substantially lowered near the surface by the negative charge. On the other hand, the deposition of positive charge on the surface of a virgin sample has no observable effect, which implies that the grain-boundary barrier near the surface of an undisturbed sample is not substantially lower than in the bulk. The barrier near the surface may instead be higher, of course, but the fraction of the total current-carrying area affected is small enough to be neglected in this case.

It is observed in Figs. 8 and 9, and also in Fig. 12, that the exposure of the samples to optical illumination substantially reduces the diffusion potential at the grain boundary. Comparing B-6 and B-10 in Fig. 9 shows that the grain boundary with the larger V_{d0} (B-10) exhibits a much greater sensitivity to illumination. These effects were predicted earlier[21,22] and may be understood by considering the effects of photogenerated minority carriers (electrons) which are attracted to the grain boundary by the electric field in the adjacent space-charge regions. Electrons accumulate at the grain boundary until their concentration reaches the magnitude at which their capture by the interface states exactly balances the supply by photogeneration within a diffusion length on either side of the grain boundary. Provided this electron concentration (which increases approximately linearly with photogeneration rate) is sufficiently large that $n\sigma_n \simeq p\sigma_p$ (σ_n, σ_p are the capture cross sections of grain-boundary interface states for electrons and holes) the interface charge Q_{is} will decrease.[21,22] More interface states will be occupied by electrons than under dark conditions, and V_d will decrease below its dark value V_{d0}. The effect is reduced in B-6 because the lower V_{d0} implies a larger p, which requires a larger n (higher optical intensity) to meet the $n\sigma_n \simeq p\sigma_p$ condition.

The results of Fig. 12 further indicate that, for each order-of-magnitude change in the photogeneration rate, the value of V_d for $V=0$ decreases by approximately 0.07 eV. Since the majority-carrier concentration at the grain boundary $p \sim \exp(-V_d/V_T)$ and $V_T = 0.026$ V at 300 K, we expect approximately an order-of-magnitude increase in this concentration. This observation is consistent with our earlier theoretical work, and confirms that for appreciable photogeneration, $n\sigma_n \approx p\sigma_p$ at the grain boundary.[21] This condition implies a charge in grain-boundary interface states which is modified by the photogeneration in such a way that the decrease in diffusion potential ΔV_d is one half of the quasi-Fermi-level separation $\Delta E_F = E_{Fn} - E_{Fp}$ at the grain boundary.[14]

Series-resistance effects from the bulk silicon grains has been found to be negligible in the data presented in Sec. V, except at the largest current densities and lowest V_{d0}. For these currents, the coalescence of the various curves at different temperature and optical-illumination intensities (Fig. 5 to 8) indicate the onset of series-resistance effects. For the nonuniform grain boundaries, this mechanism occurs at lower current densities than would be expected on the basis of a one-dimensional model of the current transport, particularly at low temperature. This is understandable since at the low temperature, the effective area of active grain-boundary conduction is small and under these conditions, the series resistance increases and is explained in terms of a spreading resistance calculation.

Additional support for the notion of characteristic interface defects (a peak in N_{is} near midgap) comes from a consideration of the crystal mismatch at the grain boundary. Let us consider this mismatch on the basis of a simple model such as that of Fig. 17. This represents a realistic mismatch angle for grain boundaries in cast silicon. Note that characteristic defects are periodically repeated along the grain-boundary plane but at distances of many atomic spacings. In the vertical direction, the repetition distance will be much shorter, the dimension of a unit cell. It is clear that not all of these defect sites contribute interface states near midgap (which would correspond to unsatisfied bonds) since $\int N_{is} dE \simeq 10^{15}$–$10^{16}$ m^{-2} over the energy range corresponding to the midgap peak, whereas the total density of atoms on the boundary plane is 10^3–10^4 times larger. This assumes that the orientational mismatch between adjacent grains is preserved over macroscopic distances.[23]

It is interesting to also note that, by virtue of the periodic nature of the defect structure, a two-dimensional *band* conduction should be possible in the grain-boundary plane. These bands will be rather narrow for momentum parallel to the page in Fig. 17 as a result of the repetition length being several atomic distances, but could be wide for transport in the perpendicular direction.

With regard to the oscillations reported in Sec. V, we believe these to be due to electric-field-enhanced emission from the localized interface states at the grain boundary.

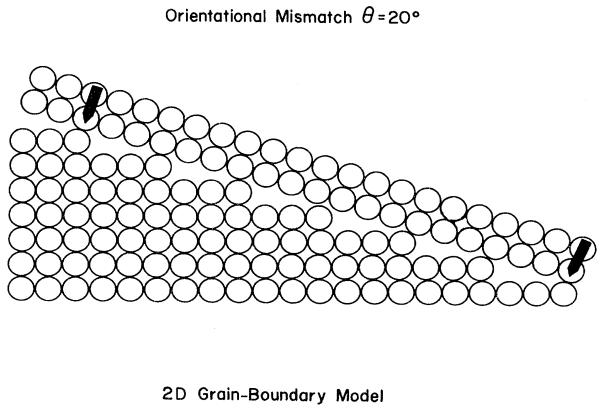

FIG. 17. Periodic nature of defect structure is suggested by this two-dimensional (2D) model. Note repetition of approximately equal disorder structure with a period of three atomic spacings along the interface between the two crystals. True periodicity is indicated by the arrows.

The beneficial effect of increased temperature supports this view, as it would provide for thermally assisted field emission. An alternative explanation which we considered for a time was impact ionization in the localized regions of high electric field that are expected from the spatial nonuniformity of the grain-boundary potentials, but this would be expected to display a negative temperature coefficient. The oscillations appear to reflect the periodic emptying and filling of the interface states with charge, which in turn affects the electric-field distribution. As the states capture holes, the field ξ_{m2} on the reverse-biased side of the boundary is enhanced, and at a particular value, the emission rate increases rapidly. Having released their charge, ξ_{m2} decreases, quenching the emission and refilling of the states begins again.

The relative orientations of the crystals on either side of the interface of sample (B10) of Figs. 5, 8, and 10–12 were measured using x-ray precession photography.[24] The crystals were found to have a 9° mismatch of the (111) planes, and the grain-boundary plane bisected this mismatch angle. These mismatch angles were typical of electrically active grain boundaries in the silicon material studied in this paper.

VIII. CONCLUSIONS

On the basis of the experimental studies described in this paper, and the theoretical arguments concerning the collection velocity for majority carriers of the grain boundary, the rate-limiting process of majority-carrier supply by diffusion to the grain boundary should be incorporated into any transport model. The thermionic emission theory used by previous authors is expected to provide at best an order-of-magnitude estimate of the current across the electrically-biased grain boundary. Grain boundaries with a variety of diffusion potentials exist[25] in Wacker "Silso" silicon, and many of these boundaries contain potential barriers which are spatially nonuniform over macroscopic portions of the grain-boundary plane. Spatially uniform grain boundaries also exist in this material, and for these samples a reasonable agreement with the theoretical one-dimensional model is obtained. Grain-boundary interface-state densities measured in this material are in the range of 10^{15}–10^{16} $m^{-2}eV^{-1}$ and exhibit an increase with energy away from E_v in the lower half of the energy gap between 0.3 and 0.5 eV. More direct measurements of these interface-state distributions, such as depleted-layer spectroscopy techniques[26] are necessary for accurate determinations, since the results are otherwise transport-model dependent. An adequate understanding of grain-boundary phenomena in cast silicon materials, or vapor-deposited polycrystalline thin films, will challenge research workers for some time to come.

ACKNOWLEDGMENTS

It is a pleasure to acknowledge helpful discussions with Kwan Kao, Lex De Groot, and Alvin Wexler (University of Manitoba), Wei Hwang, Edward Yang, and Ed Poon (Columbia University), and Paul Panayotatos (Rutgers University) on topics described in this paper, and Frank Hawthorne (University of Manitoba) for conducting the x-ray precession photography. The financial support of the Natural Sciences and Engineering Research Council of Canada (NSERC) provided under strategic Grant No. G0442 and operating Grant No. A1330 are also very much appreciated.

APPENDIX A: NUMERICAL ANALYSIS OF GRAIN BOUNDARIES

The general semiconductor transport problem, neglecting quantum-mechanical effects such as reflection by the grain-boundary interface, is solved self-consistently with the following equations.

Poisson's equation relates the charge distribution to the electrostatic potential. This may be expressed as

$$\nabla^2\phi_i = -\frac{\rho}{\epsilon} , \tag{A1}$$

where ϕ_i is the electrostatic potential, ϵ is the permittivity of the semiconductor, and ρ is the charge density given by

$$\rho = q(p - n + N_d^+ - N_a^-) + Q_{is} . \tag{A2}$$

In Eq. (A2), Q_{is} is the net charge in the grain-boundary interface states (assumed in our results to be independent of n and p, and hence of bias voltage) and N_d^+, N_a^- are the ionized donor,acceptor impurity concentrations. We also have the current-density expressions[17]

$$\vec{J}_n = q\mu_n n\vec{\xi} + qD_n\vec{\nabla}n = \mu_n n\vec{\nabla}E_{Fn} , \tag{A3}$$

$$\vec{J}_p = q\mu_p p\vec{\xi} - qD_p\vec{\nabla}p = \mu_p p\vec{\nabla}E_{Fp} , \tag{A4}$$

and current continuity equations

$$\frac{\partial n}{\partial t} = G - U + \frac{1}{q}\vec{\nabla}\cdot\vec{J}_n , \tag{A5}$$

$$\frac{\partial p}{\partial t} = G - U - \frac{1}{q}\vec{\nabla}\cdot\vec{J}_p , \tag{A6}$$

where G is the generation rate and U is the net recombination rate. For simplicity, we shall restrict ourselves to the steady state ($dn/dt = dp/dt = 0$), and in the bulk of the semiconductor, we have employed the usual recombination model,[17]

$$U = \left[\frac{1}{\tau}\right]\frac{pn - n_i^2}{p + n + 2n_i} , \tag{A7}$$

with $\tau = (\sigma v_{th} N_t)^{-1}$ as the bulk lifetime for minority carriers.

1. Program formulation

A nonuniform, one-dimensional mesh (of 61 nodes) was constructed to simulate an isolated grain boundary in p-type silicon. The boundary is situated at $x = 0$, and 20 μm of bulk semiconductor is allowed on either side. Guided by the depletion approximation, one expects a space-charge region on the order of 1 μm for the doping concentration considered in this paper. Hence elements are more densely packed near the boundary than in the bulk material. Dirichlet boundaries (i.e., those of a fixed, known po-

tential) are enforced at the regions' edges and the grain boundary is modeled as an interior Neumann interface. The current density is evaluated from

$$\vec{J}=\vec{J}_n+\vec{J}_p=-q(\mu_n n\vec{\nabla}\phi_n+\mu_p p\vec{\nabla}\phi_p)\ , \tag{A8}$$

with the use of the quasi-Fermi-*potentials* $\phi_n=-E_{Fn}/q$ and $\phi_p=-E_{Fp}/q$. The gradients of ϕ_n and ϕ_p are determined by numerical differentiation.

2. Finite-element modeling techniques

In order to efficiently simulate the transport processes associated with semiconductor materials, one requires a model which is both physically accurate and numerically stable. Previous researchers have successfully applied variations of the finite-difference[29,30] and finite-element[31] methods to a number of semiconductor problems. Unfortunately, many of the earlier techniques suffer from lack of generality (e.g., restricted forms of carrier transport) and limited accuracy of solutions.

The method presented here uses quadratic, isoparametric elements together with a fully implicit Newton-Raphson algorithm to achieve accurate Fermi potentials with acceptable computational effort. Although the grain-boundary examples cited within this paper are analyzed in one spatial dimension, the method is equally suited for two- and three-dimensional analysis.

The electronic transport processes describing the behavior of a semiconductor device may be reduced to a set of three simultaneous, nonlinear, Poisson-type equations. A variational scheme is applied along with finite-element discretization to generate a quasilinear system of equations which is then transformed into a suitable residual vector. The final solution to the transport equations is obtained by zeroing that residual vector via Newton's algorithm. The following discussion describes the finite-element method in a very superficial manner. Interested readers are referred to Refs. 32—34 for related mathematical proofs and a more detailed explanation of the technique.

3. The finite-element method

Consider

$$L\phi=-\vec{\nabla}\cdot(\epsilon\vec{\nabla}\phi)=\rho\ , \tag{A9}$$

where, for the moment, the medium ϵ and source ρ are assumed to be functions of position but independent of the potential ϕ. It can be shown that under suitable boundary conditions, the energy functional,

$$F=\langle L\phi,\phi\rangle-2\langle\phi,\rho\rangle\ , \tag{A10}$$

is minimized by the solution of (A9). The triangular brackets denote a suitably defined inner product. Under influence of the Dirichlet,

$$\phi\,|_s=g(s)\ , \tag{A11}$$

and Neumann,

$$\hat{n}\cdot(\epsilon\vec{\nabla}\phi)\,|_s=h(s)\ , \tag{A12}$$

boundary conditions, together with the interface condition,

$$\hat{n}\cdot(\epsilon_1\vec{\nabla}\phi-\epsilon_2\vec{\nabla}\phi)\,|_i=k(i)\ , \tag{A13}$$

the functional may be explicitly written as

$$F=\int_R\epsilon(\vec{\nabla}\phi)^2-2\phi\rho\,d\Omega -2\int_{S_0}\phi h\,ds-\int_{S_i}\phi k\,ds\ . \tag{A14}$$

Providing ϵ is strictly positive, the operator L will be positive-definite. Choosing a suitable basis set $\underline{\alpha}$ and writing

$$\phi=\underline{\phi}^T\underline{\alpha}=\underline{\alpha}^T\underline{\phi}\ , \tag{A15}$$

$$\rho=\underline{\rho}^T\underline{\alpha}=\underline{\alpha}^T\underline{\rho}\ , \tag{A16}$$

$$\epsilon=\underline{\epsilon}^T\underline{\alpha}=\underline{\alpha}^T\underline{\epsilon}\ , \tag{A17}$$

leads to the matrix equation

$$(S^*\underline{\epsilon})\underline{\phi}=B\underline{\rho}\ , \tag{A18}$$

or

$$S\underline{\phi}=\underline{b}\ , \tag{A19}$$

where

$$S^*=\int[(\vec{\nabla}\underline{\alpha})\cdot(\vec{\nabla}\underline{\alpha}^T)]\underline{\alpha}^T d\Omega\ , \tag{A20}$$

$$B=\int\underline{\alpha}\,\underline{\alpha}^T d\Omega\ , \tag{A21}$$

and superscript T refers to the transpose of the column vectors. If the basis set is selected to cover only small regions of space in a piecewise-continuous fashion (i.e., a finite element) then the local matrices S and B may be accumulated on an element-by-element basis to form a large, sparse global system matrix. The actual shape functions to be integrated are generated via an isoparametric transformation in order to cover deformed regions of space.[35]

4. The Newton-Raphson algorithm

We now shall relax the restriction requiring the source and medium to be independent of the potential. To solve

$$\underline{R}=S\underline{\phi}-\underline{b}=\underline{0}\ , \tag{A22}$$

the iterative sequence

$$J^n(\underline{\Delta\phi})^{n+1}=\underline{R}^n\ , \tag{A23}$$

where

$$(\underline{\Delta\phi})^{n+1}=\underline{\phi}^n-\underline{\phi}^{n+1}\ , \tag{A24}$$

will converge quadratically for a suitable starting estimate of the potential vector.[36] The Jacobian matrix is given as

$$J_{ij}^n=\frac{\partial R_i^n}{\partial\phi_j^n}=S_{ij}^n+\left[S_{ilJ}^*\left[\frac{\partial\epsilon_j^n}{\partial\phi_j^n}\right]\right]\phi_1^n-B_{ij}\left[\frac{\partial\rho_j^n}{\partial\phi_j^n}\right]\ , \tag{A25}$$

and is reevaluated at each step in the iterative sequence.

Note that as ϵ and ρ are explicitly known functions of potential, the Jacobian is easily calculated. One should also observe that although S is sparse and symmetrical, J is sparse (and of the same topology as S) but asymmetrical. Furthermore, the structure of J does not change as the iterations proceed and, provided J is nonsingular, the final solution is independent of the Jacobian.

When three equations are involved, the potentials may be combined into a single, complex vector with the resulting matrix equation

$$\begin{bmatrix} \frac{\partial R_i}{\partial \phi_i} & \frac{\partial R_i}{\partial \phi_n} & \frac{\partial R_i}{\partial \phi_p} \\ \frac{\partial R_n}{\partial \phi_i} & \frac{\partial R_n}{\partial \phi_n} & \frac{\partial R_n}{\partial \phi_p} \\ \frac{\partial R_p}{\partial \phi_i} & \frac{\partial R_p}{\partial \phi_n} & \frac{\partial R_p}{\partial \phi_p} \end{bmatrix}^n \begin{bmatrix} \underline{\Delta\phi_i} \\ \underline{\Delta\phi_n} \\ \underline{\Delta\phi_p} \end{bmatrix}^{n+1} = \begin{bmatrix} \underline{R_i} \\ \underline{R_n} \\ \underline{R_p} \end{bmatrix}^n . \quad \text{(A26)}$$

As before, the local matrix expressions are accumulated (element by element) into a sparse system matrix.

During each iteration of (A26) a large sparse system of linear equations must be solved. The method chosen for this task relies on obtaining a bifactored form of the inverse.[37] The program package ASYMPAK (Ref. 38) incorporates such an algorithm while allowing the user to ignore details of the matrix structure. With this procedure, convergence is usually achieved in three to four iterations for each step of the current-voltage curve being generated.

APPENDIX B: DERIVATION OF γ AND ESTIMATION OF ITS MAGNITUDE FOR PRESENT GRAIN-BOUNDARY SAMPLES

The relationship between dV_{d0}/dT and $d\phi_p/dT$ for a uniform grain boundary is expressed by Eq. (11) as follows:

$$\frac{dV_{d0}}{dT} = -\gamma \frac{d\phi_p}{dT} . \quad \text{(B1)}$$

We now derive γ in terms of the interface-state density N_{is} at the grain boundary. With the use of Eq. (16),

$$\frac{dQ_{is}}{dT} = -\frac{d(Q_1+Q_2)}{dT} , \quad \text{(B2)}$$

$$qN_{is}\frac{d\phi_b}{dT} \simeq -\frac{d(Q_1+Q_2)}{dV_{d0}}\frac{dV_{d0}}{dT} , \quad \text{(B3)}$$

for $V_1=V_2=0$ and $V_{d0} \gg V_T$. Also, from the fact that $\phi_b = V_{d0}+\phi_p$,

$$qN_{is}\left[\frac{d\phi_p}{dT}+\frac{dV_{d0}}{dT}\right] \simeq -\frac{d(Q_1+Q_2)}{dV_{d0}}\frac{dV_{d0}}{dT} , \quad \text{(B4)}$$

$$\frac{dV_{d0}}{dT} = -\frac{1}{1+\frac{d(Q_1+Q_2)}{dV_{d0}}\frac{1}{qN_{is}}}\frac{d\phi_p}{dT} . \quad \text{(B5)}$$

Comparing Eqs. (B5) and (11) we have that

$$\gamma = \frac{1}{1+\frac{d(Q_1+Q_2)}{dV_{d0}}\frac{1}{qN_{is}}} . \quad \text{(B6)}$$

In order to evaluate γ for our samples, we employ Eqs. (10) and (11) for Q_1 and Q_2 from which we obtain

$$\frac{d(Q_1+Q_2)}{dV_{d0}} = -[2q\epsilon N_a(V_{d0}-V_T)]^{1/2}2q\epsilon N_a$$

$$= -\left[\frac{2q\epsilon N_a}{V_{d0}-V_T}\right]^{1/2}$$

For example, in our sample B-10, $N_a = 3\times10^{21}$ m^{-3}, $\epsilon = 11.8\epsilon_0$, $V_{d0} \simeq 0.32$ V, and $N_{is} \simeq (6-8)\times10^{15}$ m^{-2}eV^{-1} at the equilibrium Fermi-level position ($\simeq E_v + 0.5$ eV) from which we obtain $\gamma \simeq 0.6$.

[1] T. Surek, A. P. Arietedjo, G. C. Cheek, R. W. Hardy, J. B. Milstein, and Y. S. Tsuo, in *Proceedings of the 15th IEEE Photovoltaics Specialist Conference, Kissimmee, Fla., 1981,* edited by C. J. Bishop (IEEE, New York, 1981), p. 1251.

[2] C. H. Seager, G. E. Pike, and D. S. Ginley, Phys. Rev. Lett. 43, 532 (1979).

[3] G. E. Pike and C. E. Seager, J. Appl. Phys. 50, 3414 (1979).

[4] C. H. Seager and G. E. Pike, Appl. Phys. Lett. 35, 709 (1979).

[5] C. H. Seager, J. Appl. Phys. 52, 3960 (1981).

[6] H. F. Mataré, *Defect Electronics in Semiconductors* (Wiley, New York, 1971).

[7] C. R. Crowell and S. M. Sze, Solid State Electron. 9, 1035 (1966).

[8] B. R. Gossick, Solid State Electron. 6, 445 (1963).

[9] E. H. Rhoderick, J. Phys. D 5, 1920 (1972).

[10] R. Stratton, Proc. Phys. Soc. London Ser. B 69, 513 (1956).

[11] D. J. Thomson, S. R. Mejia, and H. C. Card, J. Power Sources 7, 191 (1981).

[12] J. W. Seto, J. Appl. Phys. 46, 5247 (1975).

[13] G. Baccarini, B. Ricco, and G. Spadini, J. Appl. Phys. 49, 5565 (1978).

[14] H. C. Card, J. Appl. Phys. 52, 3671 (1981).

[15] W. E. Taylor, N. H. Odell, and H. Y. Fan, Phys. Rev. 88, 867 (1952).

[16] N. D. Arora, J. R. Hauser, and D. J. Roulston, IEEE Trans. Electron Devices ED-29, 292 (1982).

[17] S. M. Sze, *Physics of Semiconductor Devices,* 2nd Ed. (Wiley, New York, 1981), pp. 37 and 248.

[18] D. J. Thomson and H. C. Card, J. Appl. Phys. 54, 1976 (1983).

[19] L. Kazmerski, *Polycrystalline and Amorphous Thin Films and Devices* (Academic, New York, 1980).

[20] Y. W. Lam, M. A. Green, and L. W. Davies, Appl. Phys. Lett. 37, 1087 (1980).

[21] H. C. Card and E. S. Yang, IEEE Trans. Electron Devices ED-24, 397 (1977).

[22] P. Panayotatos and H. C. Card, IEEE Electron Devices Lett. EDL-1, 263 (1980).

[23]O. L. Krivanek, S. Isoda, and K. Kobayashi, Philos. Mag. 36, 931 (1977).

[24]M. J. Buerger, *The Precession Method in X-Ray Crystallography* (Wiley, New York, 1966).

[25]D. Redfield, Appl. Phys. Lett. 38, 174 (1981).

[26]G. L. Miller, D. V. Lang, and L. C. Kimmerling, Ann. Rev. Mat. Sci. 7, 377 (1977).

[27]C. H. Seager, in *Grain Boundaries in Semiconductors* (North-Holland, New York, 1982), p. 85, and references to their early work within.

[28]J. Werner, W. Jantsch, K. H. Froehner, and H. J. Queisser, in *Grain Boundaries in Semiconductors,* Ref. 27, p. 99.

[29]M. S. Adler, in *Numerical Analysis of Semiconductor Devices,* edited by B. T. Browne and J. J. Miller (Boole, Dublin, 1979), p. 3.

[30]K. Kani, in *Numerical Analysis of Semiconductor Devices,* Ref. 29, p. 104.

[31]P. E. Cottrell and F. M. Buturla, in *Numerical Analysis of Semiconductor Devices,* Ref. 29, p. 31.

[32]S. G. Mikhlin, *Variational Methods in Mathematical Physics* (Pergamon, Oxford, 1964).

[33]A. Wexler, Report TR80-4, Department of Electrical Engineering, University of Manitoba, Winnipeg, Canada (unpublished).

[34]O. C. Zienkiewicz, *The Finite Element Method in Engineering Science* (McGraw-Hill, London, 1971).

[35]A. Wexler, in *International Conference on Finite Elements* in *Water Resources Part II, Princeton, New Jersey,* edited by W. G. Gray, G. F. Pinder, and C. A. Brebbia (Publisher, City, Year), p. 2.3.

[36]A. Roger, IEEE Trans. AP-29, 232 (1981).

[37]K. Zollenkopf, in *Large Sparse Sets of Linear Equations,* edited by J. K. Reid (Academic, New York, 1971), p. 75.

[38]J. G. Shaw and A. Wexler, Report TR79-4, Deptartment of Electrical Engineering, University of Manitoba, Winnipeg, Canada (unpublished).

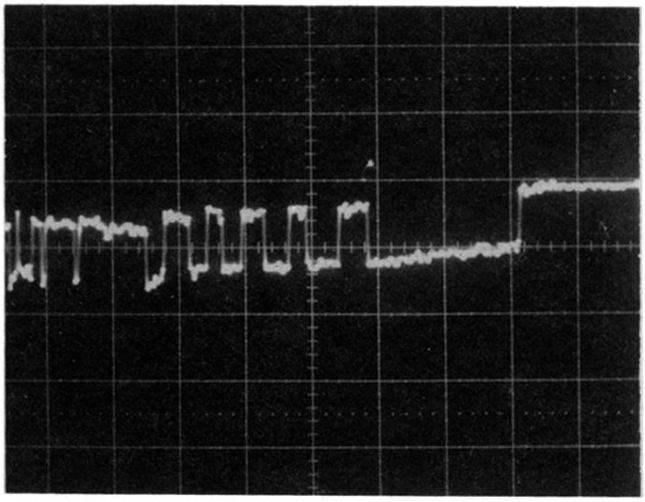

FIG. 13. Current oscillations observed at high dc current densities. Grain-boundary sample B-11. $V=15$ V; $I=150$ mA. Vertical scale: 500 μA/division. Horizontal scale: 1 ms/division.